Geomechanics and Engineering, *Vol. 29, No. 2 (2022) 155-170*
https://doi.org/10.12989/gae.2022.29.2.155

Seismic loading response of piled systems on soft soils – Influence of the Rayleigh damping

Guillermo A. López Jiménez[1], Daniel Dias*[2,3] and Orianne Jenck[1]

[1]*Univ. Grenoble Alpes, CNRS, Grenoble INP**, 3SR, F-38000 Grenoble, France*
[2]*Hefei University of Technology, School of Automotive and Transportation Engineering, Hefei, China*
[3]*Antea Group, Paris, France*

(Received October 28, 2021, Revised February 14, 2022, Accepted March 4, 2022)

Abstract. An accurate analysis of structures supported on soft soils and subjected to seismic loading requires the consideration of the soil-foundation-structure interaction. An important aspect of this interaction lies with the energy dissipation due to soil material damping. Unlike advanced constitutive models that can induce energy loss, the use of simple elastoplastic constitutive models requires additional damping. The frequency dependent Rayleigh damping is a formulation that is frequently used in dynamic analysis. The main concern of this formulation is the correct selection of the target damping ratio and the frequency range where the response is frequency independent. The objective of this study is to investigate the effects of the Rayleigh damping parameters in soil-pile-structure and soil-inclusion-platform-structure systems in the presence of soft soil under seismic loading. Three-dimensional analyses of both systems are carried out using the finite difference software Flac3D. Different values of target damping ratios and minimum frequencies are utilized. Several earthquakes are used to study the influence of different excitation frequencies in the systems. The soil response in terms of accelerations, displacements and strains is obtained. For the rigid elements, the results are presented in terms of bending moments and normal forces. The results show that when the frequency of the input motion is close to the minimum (central) frequency in the Rayleigh damping formulation, the overdamping amount is reduced, and the surface spectral acceleration of the analyzed pile and inclusion systems increases. Thus, the bending moments and normal forces throughout the piles and inclusions also increase.

Keywords: dynamic analysis; numerical modelling; Rayleigh damping; rigid inclusion; pile

1. Introduction

The pile foundation has been used for a long time, especially in the presence of soft soils, to support buildings, bridges, highways, as well as railways. The accurate analysis of these structures, when subjected to seismic loadings, requires the consideration of the soil-foundation-structure interaction. This interaction permits considering simultaneously the load transfer mechanisms and relative movements.

The rigid inclusion system is a method similar to the pile system; however, in this technique, the rigid elements are separated from the structure by the presence of an earth platform. The arching effect in the platform allows transferring part of the load to the rigid elements. The remained load is directly transmitted to the soft soil. The dissipation of energy in the platform represents a great advantage in the case of active seismic zones. Both pile and rigid inclusion systems, presented in Fig. 1, increase the bearing capacity and permit the reduction of the settlements.

The substructure and direct method are two different ways to evaluate the soil-foundation-structure systems. In the substructure method, the inertial and kinematic effects are studied separately (Stewart *et al.* 1999). This technique has been utilized by Han (2001), Maheshwari *et al.* (2004), Tokimatsu *et al.* (2005), Kim *et al.* (2015) and, Messioud *et al.* (2016). On the other side, in the direct method, all the elements of the system (soil, foundation, structure and connections) can be analyzed in the same model in a single step accounting for both inertial and kinematic interaction. Several authors have analyzed pile and inclusion systems with the direct method (Chu and Truman 2004, Hayashi and Takahashi 2004, Nghiem and Nien-Yin 2008, Carbonari *et al.* 2011, Tabatabaiefar and Fatahi 2014, Fatahi *et al.* 2014, Chatterjee *et al.* 2015, Mánica-Malcom *et al.* 2016, Nguyen *et al.* 2017, López Jiménez *et al.* 2018, Khanmohammadi and Fakharian 2018, Ghorbanzadeh *et al.* 2020).

In the direct method, the soil is discretized in a finite domain limited by artificial boundaries. These boundaries represent the semi-infinite nature of the soil and avoid reflections of the propagating waves back into the model. The dissipation of energy through the boundaries is known as radiation damping and is not an inherent property of the material. The radiation damping is complemented by the material damping that represents the loss of energy within the soil itself, mainly due to microstructural mechanisms such as inter-particle sliding, friction, structure rearrangement, and pore fluid viscosity. The material damping has been identified as one of the main factors incorporated into the study of soil-foundation-structure

*Corresponding author, Professor
E-mail: d.dias69@gmail.com

ISSN: 2005-307X (Print), 2092-6219 (Online)

interaction systems (Ambrosini 2006, Wolf 1985) because it depends on the characteristics of the soil and not on the geometry and boundaries. Hereafter, the term damping refers only to material damping.

The Rayleigh damping has been used as an alternative to represent the dissipation of energy in seismic analysis. The effective results of the Rayleigh formulation have been proved by some authors. For instance, Mánica *et al.* (2014) developed a 3D numerical seismic analysis to show the advantages and drawbacks of different damping formulations (local, Rayleigh and hysteretic) with a typical stratigraphy of Mexico city. They concluded that the Rayleigh damping is the most suitable alternative to represent the dissipation of energy in dynamic analysis. Suwal *et al.* (2014) developed several linear analyses in an idealized soil profile to explore the influence of Rayleigh damping formulation on-site response analysis. The results showed that the full Rayleigh damping formulation is consistent with the response obtained with a frequency independent analysis; however, the response using the simplified formulation is underestimated. Sun *et al.* (2019) analyzed the influence of Rayleigh damping formulation considering a visco-elastic behavior of tunnels under seismic loading. The results conclude that a safe seismic design of tunnels depends on the correct selection method to obtain the viscous damping parameters. Other authors (Hashash and Park 2002, Phillips and Hashash 2009, Phillips *et al.* 2012, Mánica *et al.* 2014, Priestley and Grant 2005, Amorosi *et al.* 2010, Wang 2011, Spears and Jensen 2012, Tsai *et al.* 2014) have studied the impact of a defective selection of the Rayleigh damping parameters on the seismic site response.

Dealing with pile and rigid inclusion systems, authors such as Wu and Finn 1997, Lu *et al.* 2005, Rangel-Núñez *et al.* 2008, Hatem 2009, Shahrour *et al.* 2012, Kumar *et al.* 2016, Luo *et al.* 2016 and Nguyen *et al.* 2017 have utilized the Rayleigh damping in their investigations. However, in most of these studies, there is no discussion about the influence of the Rayleigh damping parameters on the response of the systems (soil, vertical elements and superstructure).

Considering the above information, the main objective of this paper is not dedicated to the study of the correct selection of the damping parameters but to the investigation of the impact of these damping parameters on the response of pile and inclusion systems. To achieve this goal, a range of damping ratios and minimum frequencies are considered in the analyses of soil-pile-structure and soil-inclusion-platform-structure systems developed using the finite difference software Flac3D. When the single control frequency approach is considered in the Rayleigh formulation, the simplest approximation considers the minimum frequency equal to the frequency that corresponds to the first mode of the soil column and the damping ratio within a range of 1 to 5%.

It is important to highlight that the direct method is used in this study to represent in a realistic manner the geometrical complexity, the connection between elements, as well as the material properties in the numerical models. The idea is to cover many uncertainties that are involved in the pile and inclusion systems to obtain reliable results but without incurring in excessive time calculations. Then, use the results to provide conclusions and recommendations to be applied in other research studies or even in the practical design of engineering projects.

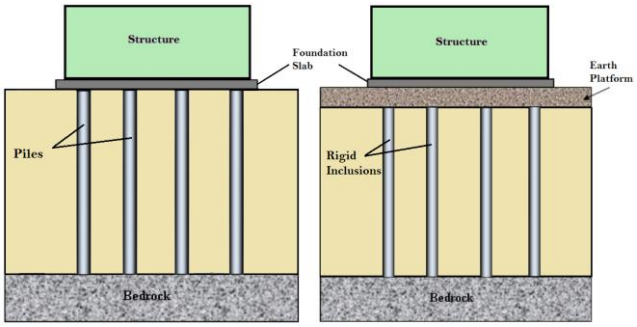

(a) Soil-Pile-Structure (b) Soil-Inclusion-Platform-Structure

Fig. 1 Vertical reinforcement systems

In the models, the behavior of soil is represented by the linear elastic perfectly plastic model with a Mohr-Coulomb shear failure criterion. This model needs additional damping for the elastic part of the response, where no energy loss occurs. The additional damping is introduced in this study by Rayleigh damping. Different earthquake input motions with different predominant frequencies are used to verify the influence of the frequency in the response of the systems. The bending moments and normal forces along the rigid inclusions and piles are compared. Accelerations, displacements and shear strains in the soil are also displayed.

1.1 Rayleigh damping

The Rayleigh damping is expressed in a matrix form and assumed proportional to the mass and stiffness matrices (Eq. (1)).

$$[\mathrm{C}] = \alpha[\mathrm{M}] + \beta[\mathrm{K}] \tag{1}$$

where [C] is the damping matrix, [M] and [K] are the mass and stiffness matrices respectively α and β are the mass-proportional and stiffness-proportional damping constants. For a multi-degree of freedom system, the critical damping ratio (ξ_i), at any natural frequency of the system (ω_i), can be calculated from the following equation

$$\alpha + \beta\omega_i^2 = 2\omega_i\xi_i \tag{2}$$

Considering Eq. (2), Fig. 2 represents the curves with only the component proportional to the mass ($\beta = 0$), the part proportional to the stiffness ($\alpha = 0$) and the curve of the sum of both components. It is evident that the curve of the sum of the components has a limited frequency range where an approximate frequency independent response can be obtained. This range is limited by a low frequency (f_0) and a large frequency (f_1). It is commonly considered f_0 as the frequency that corresponds to the first mode of the soil column, calculated by $f_n = V_s/4H$, where $\mathrm{V_s}$ is the elastic shear wave velocity and H is the thickness of the soil

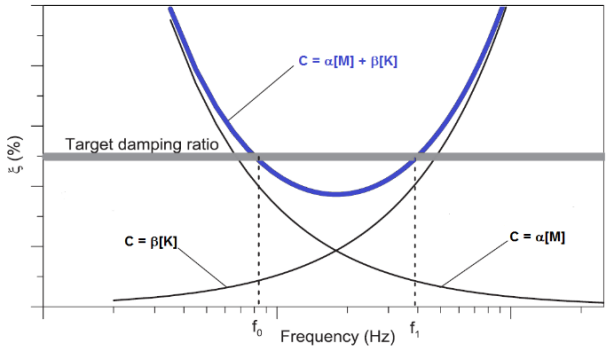

Fig. 2 Rayleigh damping formulation

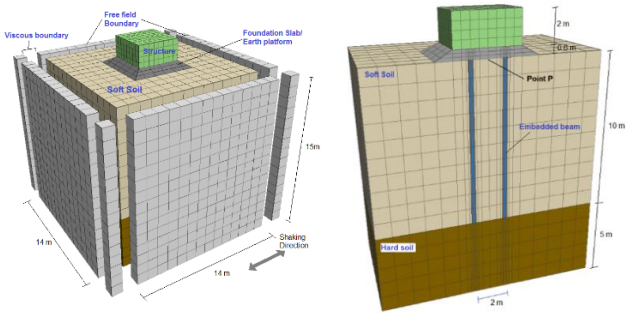

(a) 3D Model (b) Embedded beam

Fig. 3 Basic geometry of the numerical model

column. For larger frequencies, an approach known as the single control frequency considering that f_1 is equal to f_n is used (Idriss *et al.* 1975, Suwal *et al.* 2014). There are many approaches to obtain the largest frequency. The simplest considers a larger frequency that corresponds to the predominant frequency (f_p) of the input motion. Kwok *et al.* (2007) suggest a frequency equal to five times f_n. Other authors suggest a value of $f_1 = nf_n$ with n being the smallest odd integer so f_1 is greater than f_p (Hudson *et al.* 1994, Rathje and Bray 2001). The target damping level is normally taken equal to the small-strain damping or to the smallest value to guarantee the numerical stability (Kwok *et al.* 2007). The values are also dependent on the strain level induced by the earthquake (Mánica *et al.* 2014). In a rigorous sense, the target damping ratio can be determined by a one-dimensional site response analysis. However, in this study, the assigned target damping for the different soil layers is considered to be in the range of 1 to 5% as usually considered in engineering.

It is also noticeable from Fig. 2 that the curve representing the sum of both components reaches a minimum at

$$\xi_{min} = (\alpha\ \beta)^{1/2} \qquad \omega_{min} = (\alpha\ /\ \beta)^{1/2} \qquad (3)$$

These two parameters are input parameters when dealing with numerical modeling for the specification of Rayleigh damping. The frequency is in Hertz (cycle per second). In this study, the single control frequency approach is utilized which means that the minimum damping ratio (ξ_{min}) is equal to the target damping ratio (ξ_{tar}). Hereafter, both terms are used indistinctly.

The frequency dependent effects of the Rayleigh formulation are set up to cancel out at the frequencies of interest (frequency range over which the combined damping ratio is almost constant, from f_0 to f_1 in Fig. 2) in a time-domain analysis.

2. Numerical modeling and studied cases

2.1 Soil and superstructure model

The analyses are carried out using a two-layer soil profile, which consists of a horizontal 10 m thick soft soil layer over a 5 m thick hard soil layer. The dimensions of the volume of soil are 14 m x 14 m x 15 m. This model size is used to obtain reliable results with an acceptable time calculation. The model is constituted of 5,600 hexahedral zones. The discretization of the system using Flac3D (Itasca 2012) is depicted in Fig. 3.

The numerical distortion of the propagating wave can occur as a function of the modeling conditions. The frequency content of the input motion and the wave speed characteristics of the system affect the accuracy of the wave transmission. Kuhlemeyer and Lysmer (1973) suggested that the maximum spatial element size (Δl) must be smaller than the one-tenth to one-eighth of the wavelength associated with the highest frequency component of the input wave.

$$\Delta l = \frac{\lambda}{10} \qquad (4)$$

where λ is the wavelength associated with the highest frequency component that contains energy, which can be calculated from the wave speed (Eq. (5)) for elastic continuum systems

$$f = \frac{V_s}{\lambda} \qquad (5)$$

In this study, the maximum size of the elements that constitute the model is equal to 1 m. This allows applying frequencies between 0 and 5 Hz without perturbations due to zone dimensions.

The superstructure is modeled by a mass of 2 m height on a surface of 4 × 4 m². In the case of rigid inclusion systems, an earth platform or mattress of 0.60 m is placed between the structure and the rigid inclusions. In this case, the rigid inclusions are not embedded in the earth platform to prevent the amplification of the movement of the structure and the consequently moment and shear forces increment in the head (upper part) of the inclusions (Hatem 2009). In the bottom part, the piles and rigid inclusions are resting on a harder layer. This type of support condition allows flexibility and rotation of the pile avoiding excessive moments and shear forces increment at the pile tip zone (Zacek 1996, Sadek 2003). The superstructure and the mattress exert a homogeneous load of 62 kPa on the rigid inclusions. In the piled cases, this mattress is replaced by a concrete slab where the head of the piles are rigidly connected (Fig. 3 (a)).

Table 1 Parameters used for the numerical calculation

Parameter	"Pile/Inclusion", "Foundation Slab" and "Superstructure"	Mattress	Soft soil	Hard soil
Young modulus (MPa)	30000	50	10	100
Shear Modulus (MPa)	12500	19	3.8	38
Volumic Weight (kg/m³)	2500	2000	1600	2000
Damping Ratio	0.02	0.05	0.05	0.05
Cohesion (kPa)	-	50	5	5
Friction angle (°)	-	25	25	25
Wave velocity (m/s)	2237	160	50	223

The material properties of all the elements are presented in Table 1. The soil characteristics were taken from Hatem (2009), Okyay et al. (2012) Houda (2016), Messioud *et al.* (2016) and Rangel-Núñez *et al*. (2008). Similar ranges of values are considered for the soft soil parameters. Generally, field or in situ geophysical tests (crosshole, downhole, suspension logging test) are used to obtain the dynamic shear moduli at very small strain levels. However, these methods do not permit the evaluation of shear modulus at strain levels produced by strong earthquakes motions. Thus, with the objective to study the behavior of soil at great deformations, static shear moduli are used in the analyses (Shahrour *et al.* 2001, Chu and Truman 2004, Hatem 2009, Mánica-Malcom *et al.* 2016, Messioud *et al.* 2016).

The properties of the earth platform correspond to a treated soil (Okyay 2010) with an important cohesion to work in compression and extension. This cohesion value also allows increasing the strength of the soil and reducing the settlements. The platform thickness (0.6 m) allows the adequate transfer of loading to the inclusions and it guarantees that there is no great diminution of the amplification of the input motion at the base of the structure level (Hatem 2009, Messioud *et al.* 2016, Okyay *et al.* 2012). The linear elastic-perfectly plastic constitutive model with a Mohr-Coulomb shear failure criterion is used to represent the behavior of the soil and earth platform.

The material properties of all the vertical reinforcements (inclusions/piles) are the same. The Young modulus of the rigid elements considered (30 GPa) has been considered by other researchers (Nghiem and Nien-Yin 2008, Haldar and Babu 2010, Hokmabadi *et al.* 2014, Nguyen *et al.* 2017) and remains in the range of values for concrete or reinforced-concrete pile foundation (BSSC 2009, Eurocode 8 1998). The flexural and axial stiffness of the inclusions/piles are 11.9 MNm²/m and 2120.5 MN/m respectively. The behavior of the superstructure, foundation slab and piles or inclusions is considered as linear elastic.

2.2 Rigid vertical elements

Four piles were installed in the soft soil with a center to center spacing of 2 m in both directions (Fig. 3(b)). The reinforced concrete rigid elements were considered 10 m in length. The diameter of these elements was taken equal to 0.30 m. Considering these characteristics, flexible behavior of the piles with bending and translation is anticipated. The ratio between the sum of the rigid element surface areas to the total reinforced area (cover ratio) is equal to 1.7%. Similar values of cover ratio were used by Hatem (2009), Briançon *et al.* (2015), Houda (2016), Kumar *et al.* (2016), Mánica-Malcom *et al.* (2016).

The piles or inclusions were represented by solid elements with the introduction of a beam element in their center axis (Banerjee *et al.* 2014, Goh and Zhang 2017). This technique accounts for the physical cross-section of the pile. This allows obtaining more reliable displacements and bending moments along the depth of the pile than the technique which consists in only considering a beam structural finite element embedded in the soil (Kitiyodom *et al.* 2006, Wotherspoon 2006). The latter technique cannot consider the effect of pile volume. However, to avoid the modification of the pile response by the introduction of the beam elements, the flexural rigidity (Referred in Table 1) of these beam elements (EI) was reduced (Banerjee *et al.* 2014). This procedure allows determining the internal forces in the vertical reinforcements directly from the analysis and using interfaces placed at the periphery of the solid elements. A preliminary analysis was carried out to compare the pile response considering each pile modeled as solid elements combined with a beam element and considering only beam elements embedded in soil (Sadek and Shahrour 2004, Alsaleh and Shahrour 2009). In this preliminary analysis, a target damping ratio of 5% and a $f_{min} = 1.25$ Hz under the Loma Prieta earthquake is considered.

Fig. 4 shows how the shear forces and the bending moments in the rigid inclusion and pile systems are reduced for the combined system (solid elements and beam element) compared to the case where the piles are modeled using beam elements. The efforts presented correspond to the maximum values envelopes recorded during the calculation. The results indicate that there is a reduction from 57 to 61% of the maximum bending moments for the rigid inclusion case and from 38% to 53% for the pile case (Fig. 4(a)). These results are in accordance with (Kitiyodom *et al.* 2006, Wotherspoon 2006). The shear forces are very similar along the depth of the elements. Only a considerable reduction is observable in the three first depth meters (Fig. 4(b)).

The consideration of this technique (solid elements with beam element embedded) implies a reduction of the time step that results in a larger computation time. The time step is an important parameter that corresponds to real seismic

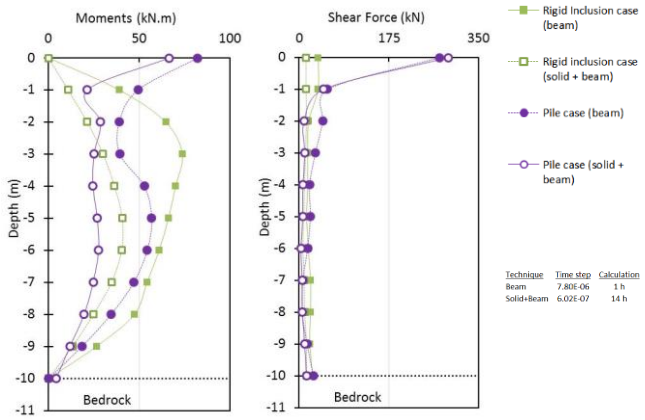

(a) Bending moments (b) Shear Forces

Fig. 4 Efforts in the pile and inclusion systems with different modeling technique

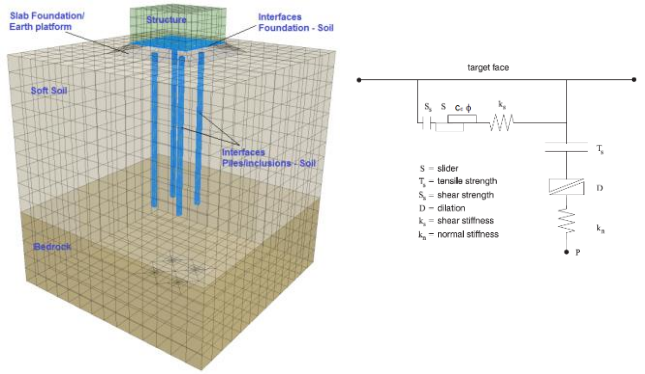

(a) Adopted interface elements (b) Components of the interface

Fig. 5 Interfaces in the numerical simulation

loading time per calculation step (Flac3D uses an explicit finite difference solution scheme). As the time step decreases, the calculation time increases. The time step for dynamic analysis is determined by the largest material stiffness and smallest zone in the model, including structural and interface elements. The time step and time calculation for both systems are also shown in Fig. 4. All the calculations were developed using a computer with a core i7 3.6Hz 64-bit processor and 8 Gigabytes of RAM.

2.3 Boundary conditions and interfaces

Artificial boundaries are utilized to represent the semi-infinite nature of the soil. Through the static modelling phases (steps), the side boundaries were fixed in their normal direction whereas the bottom part was fixed in all directions. However, these preliminary boundary conditions were changed in the dynamic analysis, the base of the model was assumed to be rigid in order to apply the acceleration input and free-field boundaries are applied on the vertical sides to avoid wave reflections (Lysmer and Kuhlemeyer 1969).

The free-field boundaries are coupled to the main grid by viscous dashpots in the normal and shear directions as follows

$$t_n = -\rho V_p v_n \quad (6)$$

$$t_s = -\rho V_s v_s \quad (7)$$

where ρ is the mass density, V_p and V_s are the velocities of the p-wave and s-wave respectively and v_n and v_s are the normal and shear components of the velocity at the boundaries respectively.

Interface elements were modeled in this study to represent the different mechanical properties of the soil and the structural elements (Maheshwari and Watanabe 2006). These elements are able to simulate the slip and detachment of the contact surface. The interface elements were set around the pile elements and between the foundation slab and the soil surface (Fig. 5(a)). The interface elements in Flac3D are presented by triangular components each one defined by three nodes and are modeled as spring-slider systems as illustrated in Fig. 5(b). The constitutive model of the interface is described by a linear Coulomb shear-strength criterion that limits the shear force acting at an interface node given by Eq. (8)

$$F_{smax} = cA + \tan\phi\,(F_n - \rho A) \quad (8)$$

where F_{smax} is the limiting shear force in the interface, F_n is the normal force, c and ϕ are the cohesion and the friction angle in the interface and A is the area is the representative area associated with the interface node. In this study, the shear strength was defined with zero cohesion and $2/3$ of the friction angle (Hazzar *et al.* 2017). As recommended by Itasca (2012) the normal and shear stiffness of the interface elements are set ten times the equivalent stiffness of the neighboring zone expressed by Eq. (9).

$$k_n = k_s = 10 \ \max\left[\frac{K + \frac{4}{3}G}{\Delta z_{min}}\right] \quad (9)$$

where K and G are the bulk and shear modulus, Δz_{min} is the smallest width of an adjoining zone in the normal direction. The values given by Eq. (9) are enough large to avoid the normal penetration and detachment on the pile-soil interface as suggested by Fan *et al*. (2007) and Rayhani and El Naggar (2008). Other authors suggested that the value of k_n should be on the order of 10^8 Pa/m.

Using the same preliminary model as in section 2.2, Fig. 6 shows the comparison of the maximal normal forces and bending moments recorded in the analysis in the rigid inclusion and pile system with and without interfaces. It is clear that the normal forces and bending moments are reduced when considering interfaces. The normal forces in the pile cases are reduced by 24% at 2 m depth when the interfaces are considered. However, this difference is reduced with depth. In the case of rigid inclusions, the reduction is smaller and equal to 12 % (Fig. 6(a)). For the bending moments, the differences are respectively of 8% and 12% for the pile and rigid inclusion systems (Fig. 6 (b)). A former parametric study for systems with different ξ_{min} and f_{min} values showed that considering a contact between pile and soil induces differences lower than 12% and largely increases the time computation (in average 8

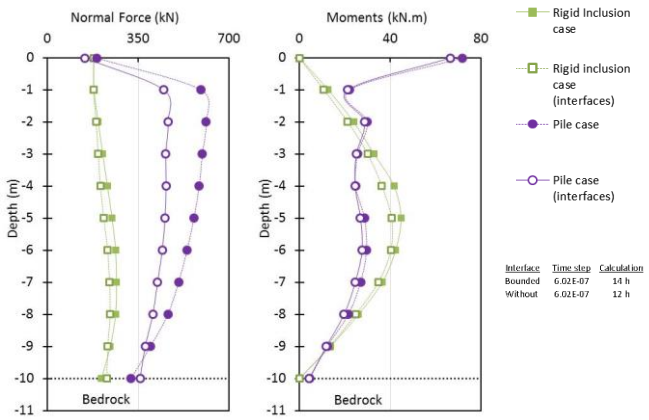

(a) Normal Forces (b) Bending Moments

Fig. 6 Efforts in the pile and inclusion systems with and without interfaces

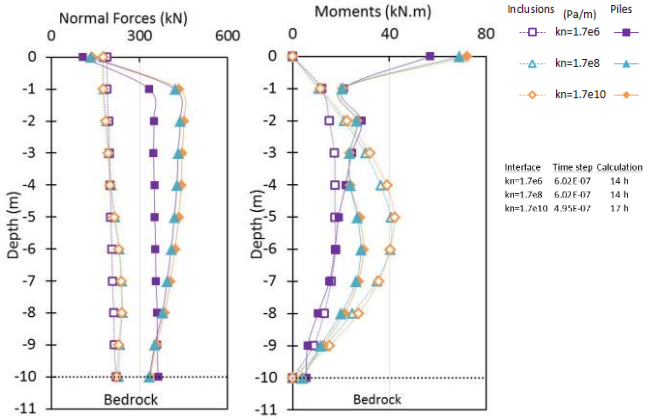

(a) Normal Forces (b) Bending Moments

Fig. 7 Efforts in the pile and inclusion systems for different k_n

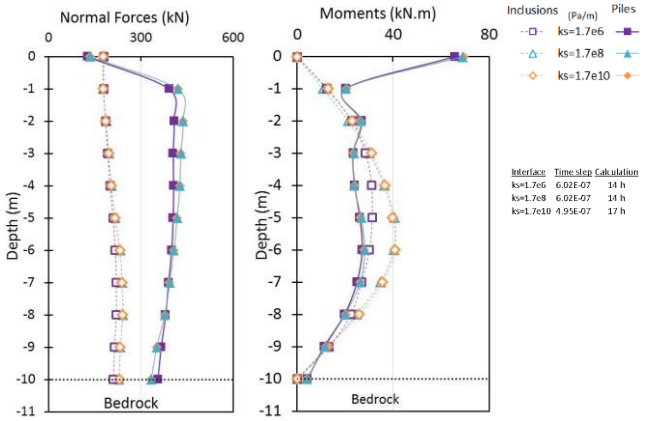

(a) Normal Forces (b) Bending Moments

Fig. 8 Efforts in the pile and inclusion systems with different k_s

hours in a computer with a core i7 3.6GHz 64-bit processor and 8 Gigabytes of RAM).

Concerning the interface parameters, the influence of the normal stiffness (k_n) and shear stiffness (k_s) is shown in Figs. 7 and 8. Generally, high values of stiffnesses should be provided to avoid movements at the interface. Fan et al. (2007) consider that a relatively larger value of normal stiffness is important to avoid normal penetration and detachment in the soil-pile interface. The studies related to the selection of k_n have shown that a larger value can simulate better the interface soil-pile (Wu *et al.* 2016, Xie *et al.* 2013). However, the increment of this value is closely related to the time step in Flac3D, which induces an increase in the time calculation. The time step for dynamic analysis is determined by the largest material stiffness and smallest zone in the model, including structural and interface elements. The efforts presented in Figs. 6 and 7 correspond to the maximum values recorded during the calculation.

It can be noted from Fig. 7 that the larger the value of k_n, the greater the normal forces and bending moments in the rigid elements. For the pile case, the normal forces obtained with a value of $k_n = 1.7e8$ Pa/m are 3% smaller than the values with $k_n = 1.7e10$ Pa/m. However, when a value of $k_n = 1.7e6$ Pa/m is utilized the normal forces are reduced by 22%. In the rigid inclusions, these forces are close, only a small decrease is observable considering the lowest value of k_n (Fig. 7(a)). These results in the inclusion systems can be explained by the transfer of surface load (distributed between the rigid inclusions and the soft soil) and the kinematic interaction between the soil and the inclusions (considering that the interface elements are able to simulate slip and detachment).

About the bending moments, the values in the rigid inclusions are almost the same for the systems analyzed with $k_n = 1.7e8$ Pa/m and $k_n = 1.7e10$ Pa/m. These values are decreased by around 54% for the system with $k_n = 1.7e6$ Pa/m. While in the piles, the values are practically the same, only in the pile head, there is a difference of 4% for the system analyzed with a smaller k_n value.The influence of k_s is lower than the influence of k_n (Fig. 8). The normal forces and moments in the piles and rigid inclusion system are practically the same. In the pile case, there is a difference of 5% for the system with $k_s = 1.7e6$ Pa/m. The bending moments along the rigid inclusions are reduced by 30% for the case with a lower k_s value (Fig. 8(b)).

3. Seismic input motion

The Loma Prieta earthquake was utilized to perform the former dynamic analyses. However, to study the influence of the input motion frequency in the systems, the Northridge and Nice earthquakes are also considered. The objective is to apply a ground motion with a greater, lower and similar predominant frequency compared to the fundamental frequency of the soil deposit. They were scaled to the same acceleration amplitude of the Loma Prieta earthquake.

The original records of each earthquake are displayed in Fig. 9. The characteristics of each earthquake are presented in Table 2. To reduce the time computation, only the highlighted 5 seconds of each accelerogram is applied to the numerical models. The selected 5 seconds is the part of

Table 2 Earthquakes base motions considered (CESMD, Grange 2008)

Earthquake	Date	Duration (s)	Peak ground acceleration PGA (m/s²)	Magnitude (Mw)	Predominant Frequency (Hz)
Loma Prieta, USA	1989/10/17	40	4.69	7.1	1.27
Northridge, USA	1994/01/17	30	8.65	6.7	4.30
Nice, France	2001/02/25	27	3.43	5.1	0.48

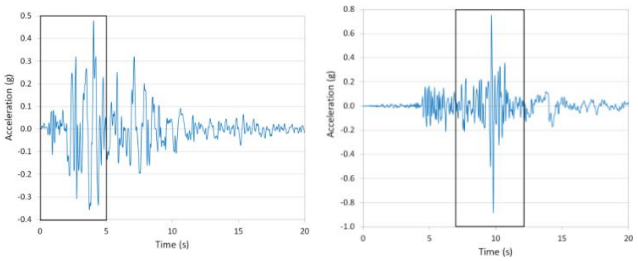

(a) Loma Prieta (b) Northridge

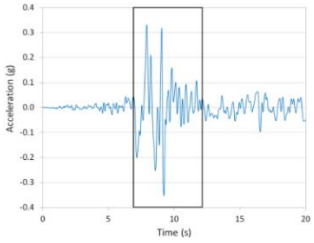

(c) Nice

Fig. 9 Original earthquakes considered in the analyses

each accelerogram considered to represent the duration of strong ground motion. Similar considerations have been presented in other studies (Rajeswari and Sarkar 2020, Mánica-Malcom *et al.* 2016, Mánica *et al.* 2014) using diverse definitions of strong motion duration.

4. Procedure of analysis

In the first step, an initial stress state is generated. Then, the vertical reinforcements are installed and the model is brought to mechanical equilibrium due to the weight of the vertical elements. The last static calculation step considers the activation of the earth platform and the surface structure. For the subsequent dynamic calculations, the absorbent and free field boundaries are added and the dynamic analyses are executed applying the corresponding horizontal wave using the accelerations (section 3) at the base of the models. The stresses and displacements obtained at the end of the static analyses were initialized which means that the results obtained are only due to the effect of the dynamic loading.

5. Numerical cases

The considered cases in this study illustrate the effect of the damping parameters in the seismic response of the soil-pile-structure and soil-inclusion-platform-structure systems.

To achieve this goal, values of 1%, 3% and 5% of the minimum damping ratio (ξ_{min}) and values from 0.3 Hz. to 4

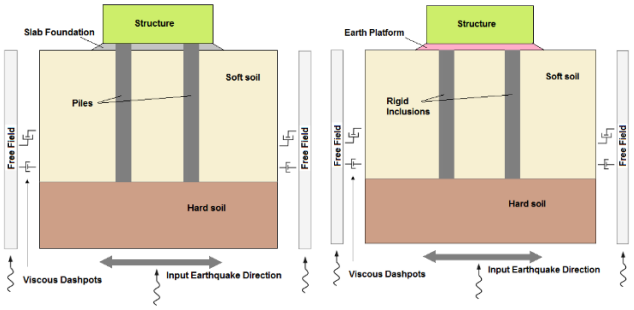

(a) Pile system (b) Rigid inclusion system

Fig. 10. Schematic representation of the analyzed systems

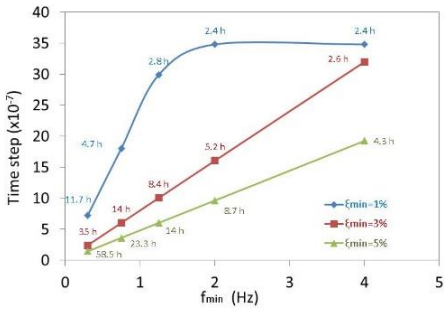

Fig. 11 Time step and calculation time for different ξ_{min} and f_{min} values

Hz. of minimum frequency (f_{min}) were utilized. The damping ratios considered are values used in this type of system under dynamic loadings (Shahrour *et al.* 2012, Kumar *et al.* 2016, Luo *et al*. 2016, Nguyen *et al*. 2017). Besides this, the damping ratio in engineering practice is usually taken as the small strain damping or the smallest value to guarantee stability (Kwok *et al*. 2007). In the case of the minimum frequencies, the considered range of values permits to cover the range of predominant frequencies of the earthquakes used in the calculations. Table 3 shows the numerical cases developed which are represented in Fig. 10. A rigid connection of the piles with the slab foundation is considered for the pile system.

In the numerical model, the structural elements represent zones where the velocity of the dynamic wave propagation is very high, this implies a very small time step when using the Rayleigh damping. For that reason, local damping with a factor of 2% is used for the superstructure and for the rigid elements. The local damping operates by adding or subtracting mass of a gridpoint or structural node at a certain time during a cycle of oscillation, keeping the overall mass of the system constant. The use of local damping is simpler than Rayleigh damping because it does damping in rigid elements has a negligible influence on the dynamic response in this type of system (Hatem 2009). Fig.

Table 3 Characteristics of the analyzed cases

System	Damping ratio ξ_{min}	Minimum frequency f_{min}	Earthquake
Rigid Inclusions	1%, 3%, 5%	0.3, 0.75, 1.25, 2.0, 4.0 (Hz)	Loma Prieta
	5%	1.25 (Hz)	Northridge, Nice
Piles	1%, 3%, 5%	0.3, 0.75, 1.25, 2.0, 4.0 (Hz)	Loma Prieta
	5%	1.25 (Hz)	Northridge, Nice

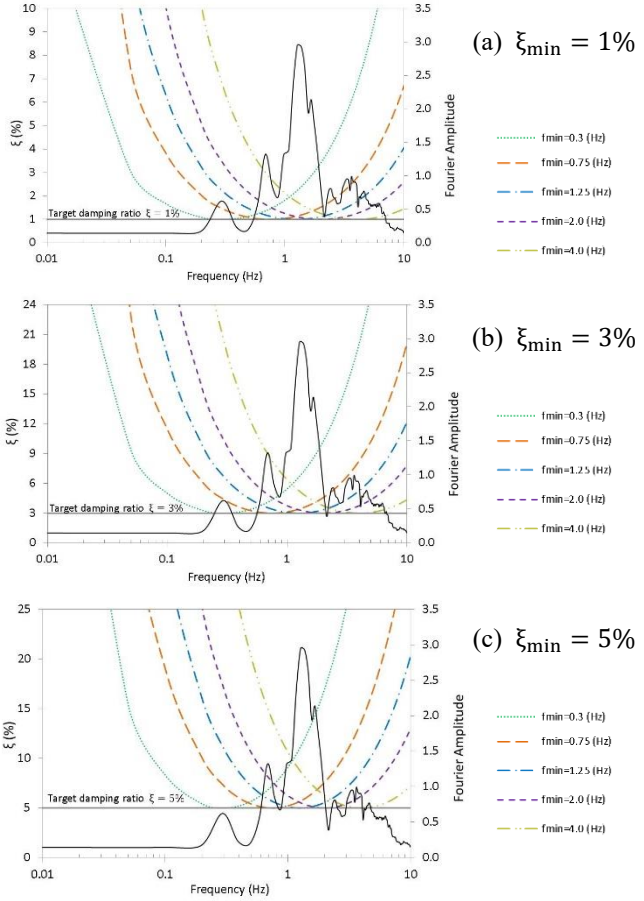

Fig. 12 Rayleigh damping formulation for different $\boldsymbol{\xi_{min}}$ and $\boldsymbol{f_{min}}$ values

11 shows the time step and time calculation for each case with different values of ξ_{min} and f_{min}

6. Results and discussion

The results of all the numerical models of Table 3 are analyzed in this part. The results are presented in terms of variation of the damping ratio for different minimum frequencies and damping ratios, acceleration and shear strains in the soil. To study the soil-structure interaction effect of each system, the spectra responses are obtained. The bending moments, normal forces and displacements along the depth of the rigid elements are compared for all cases. The efforts presented correspond to the maximum values recorded during the calculation. The comparisons in percentage are carried out using the maximum differences.

In Figs. 12 to 18, the considered input motion is the Loma Prieta earthquake.

6.1 Variation of the damping ratio

The frequency dependency of the Rayleigh damping formulation in the analyzed cases is highlighted in Fig. 12.

In this figure, the variation of the damping ratio is presented for different values of f_{min} and ξ_{tar}. The Fourier spectrum of the Loma Prieta earthquake is also displayed. The Fast Fourier Transform is used to calculate the Fourier response spectrum. The damping ratio is close to the target damping ratio when the frequency of the system is close to f_{min}. This highlights the importance of selecting carefully the position of the central frequency to capture the ground motion in the desired frequency range (frequency independent) and avoid overdamping.

For instance, from Fig. 12(a), when considering the system with 1% as the target damping and a f_{min} of 0.75 Hz, the damping ratio is close to 1%. If the minimum frequency stated is changed 1.25, 2.0 and 4.0 Hz the damping ratio increase from 1% to 1.1%, 1.5% and 2.7% respectively. Similar behavior is displayed in Fig. 12(c) when assuming $\xi_{tar} = 5\%$ and f_{min} equal to 1.25 Hz, the damping ratio is 5%, however, if the minimum frequency is modified to 2 Hz the damping ratio reaches 5.6% and 9% when the curve of f_{min} is equal to 4 Hz.

For the systems analyzed in this study, the predominant frequency of the input motion applied at the bottom of the numerical model is equal to 1.27 Hz. Due to the characteristics of the soil profile, this frequency is modified from a range of 1.13 Hz to 1.24 Hz at the surface in the analyzed cases when 5% was set as the target damping ratio. For the cases with 1% and 3% of target damping ratios, this range is from 1.18 Hz to 1.22 Hz.

6.2 Acceleration response spectra

Fig. 13 shows the calculated maximum accelerations through the section under the foundation center (Point P in Fig. 3(b)). The accelerations are greater for the systems of lower damping ratio. For instance, in the pile analyzed cases with $f_{min} = 4.0$ Hz and 1% of damping ratio, the accelerations are respectively reduced by 11% and 20% for 3% and 5% of damping ratios at the middle depth of soft soil layer (5 m depth). For the case of the rigid inclusions, the same comparison gives 8% and 19% respectively.

It can be noted that the accelerations of soil along the rigid inclusion system are greater when compared with the

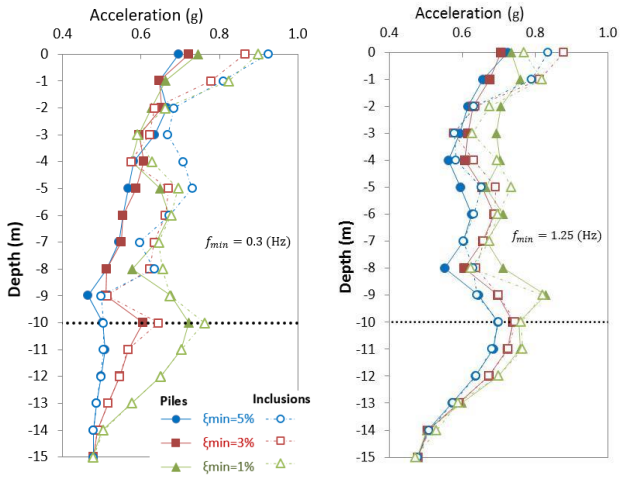

(a) $f_{min} = 0.3(Hz)$ (b) $f_{min} = 1.25(Hz)$

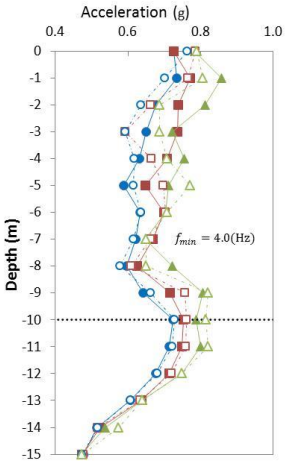

(c) $f_{min} = 4.0(Hz)$

Fig. 13 Maximum in-depth acceleration in the pile and inclusion systems

pile system for all the analyzed cases. This is clearer in the case where $f_{min} = 0.3$Hz, the accelerations are 5% to 19% greater than the respective pile system with the same target damping ratio. In the cases where $f_{min} = 1.25$ Hz and $f_{min} = 4.0$ Hz, this difference range is reduced from 5% to 13%. This can be explained by the difference in the interaction of the pile and rigid inclusion elements with the surrounding soil in each system.

It is important to highlight the significant amplification of the accelerations in presence of soft soils. It is evident from Fig. 13 that the wave propagation from the input motion acceleration (bottom part of the model) to the surface leads to a peak acceleration of 0.74 g and 0.92 g for the pile and rigid inclusion systems respectively. These values implies an amplification factor of 1.58 and 1.95 respectively over the peak input acceleration (0.47 g). Mánica *et al.* (2014) and Amorosi *et al.* (2010) obtained amplification factors around 2.2 and 1.2 respectively. Both authors considered soft clay in their studies.

To examine the influence of the soil-structure interaction in the numerical model, the acceleration response spectra of the motions recorded at the soil surface (base of the structure) are shown in Fig. 14. The response spectra are computationally calculated using a time-stepping procedure based on the interpolation of the excitation function. In all cases, the soil fundamental period and the spectral acceleration increase with respect to the spectrum of the input motion. This is significant when the period of the ground motion matches the period of the superstructure (Seed *et al.* 1988).

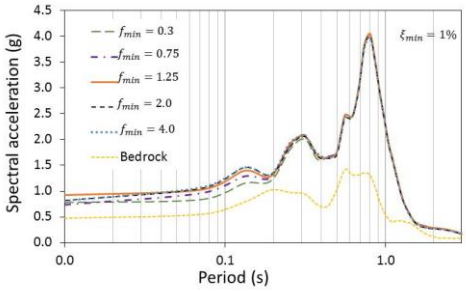

(a) $\xi_{min} = 1\%$

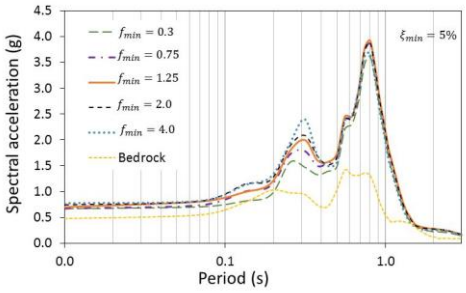

(b) $\xi_{min} = 5\%$

Fig. 14 Surface response spectra in the pile systems for different f_{min} values

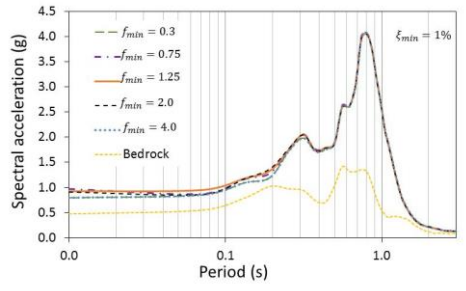

(a) $\xi_{min} = 1\%$

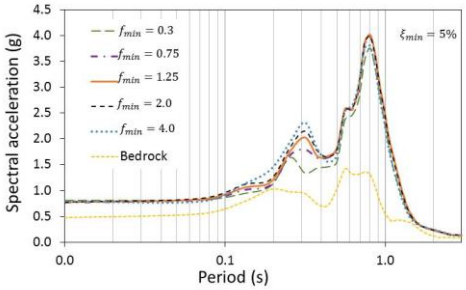

(b) $\xi_{min} = 5\%$

Fig. 15 Surface response spectra in the rigid inclusions systems for different f_{min} values

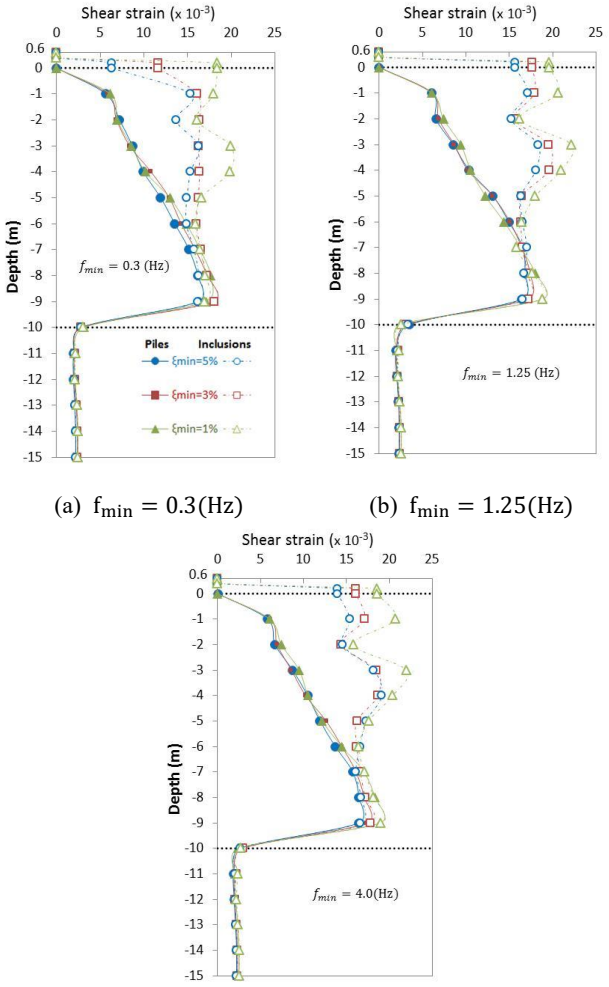

(a) $f_{min} = 0.3(Hz)$ (b) $f_{min} = 1.25(Hz)$

(c) $f_{min} = 4.0(Hz)$

Fig. 16 Maximum in-depth shear strain for the pile and rigid inclusion systems

Concerning the rigid inclusion systems, the response spectra for different values of f_{min} are similar to the pile case. However, the spectral acceleration in the rigid inclusion systems is greater than in the pile case with the same damping ratio and f_{min} (Fig. 15). This is due to the inertial interaction of the complete system and of the kinematic interaction of the vertical elements. In the case of rigid inclusions, the response spectrum was established with the surface acceleration recorded at the top of the earth platform. The acceleration at the top of the soft soil is slightly higher. This highlights the advantage of the earth platform, which dissipates energy and then reduces the inertial forces in the structure during the seismic loading.

6.3 Soil response

6.3.1 Shear strains

The maximum shear strains recorded in the center of the piled area (Point P in Fig. 3(b)) in all analyzed cases at different depths are presented in Figs. 16. It is clear that the distribution of the maximum shear amplitude is large at the top of the model (soft soil) and small at the bottom (hard

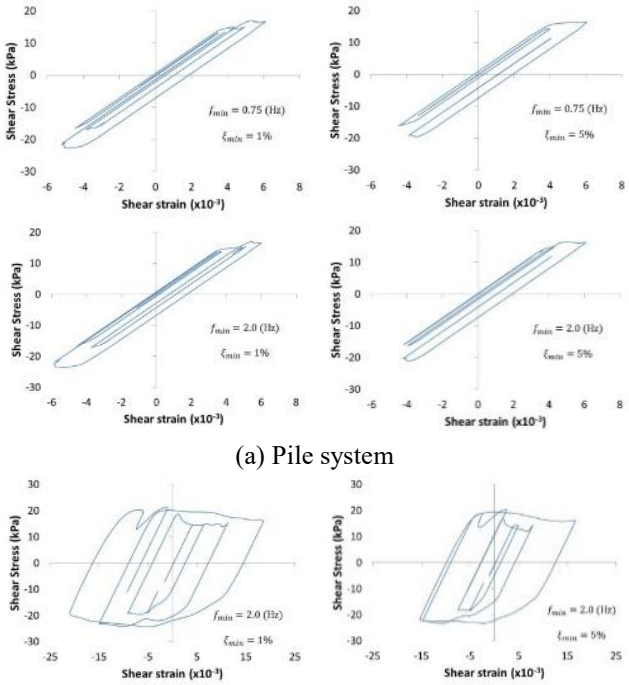

(a) Pile system

(b) Rigid inclusion system

Fig. 17 Stress strain loops in the analyzed systems with different $\mathbf{f_{min}}$ and $\boldsymbol{\xi_{min}}$

soil). It is in the upper part where the maximum damping ratio and the minimum shear stiffness are attained. This is in agreement with the results shown by Lu *et al.* (2005), Amorosi *et al.* (2010), Phillips and Hashash (2009), Tsai *et al.* (2014) and Mánica-Malcom *et al*. (2016).

It is obvious that the shear strains in the pile system are lower than the values in the rigid inclusion system at depths from 0 m to 7 m. The rigid connection of the piles with the slab foundation or the free condition in the head of the inclusions seems to have a great influence on the shear strains developed at the upper part of the models. An interesting phenomenon is observed at 2 m depth where the shear strains are importantly reduced. This can be explained by the attenuation of accelerations at this depth due to the overestimation of the damping ratio and the free condition at the head of the rigid inclusions. The shear deformations in the boundary of the hard layer and soft soil are also important due to the significant rigidity contrast between two consecutive layers (Mánica *et al*. 2014).

The maximum shear strain in the pile systems are independent of the damping ratio. However, in the rigid inclusion system, the influence of the ξ_{min} and f_{min} is important. For example, in the case where $f_{min} = 4.0$ Hz, the values with 1% of minimum damping ratio are reduced in a range from 2% to 13% with respect to the values of $\xi_{min} = 3\%$. The strains at the surface with a 5% of damping ratio increase respectively by 80% and 200% than the cases where $\xi_{min} = 3\%$ and $\xi_{min} = 1\%$.

The sketch of the stress-strain behavior computed for the cases where $f_{min} = 0.75$ Hz and $f_{min} = 2.0$ Hz for different target damping ratios are shown in Fig. 17. These diagrams were obtained at 1 m depth. It can be noted that

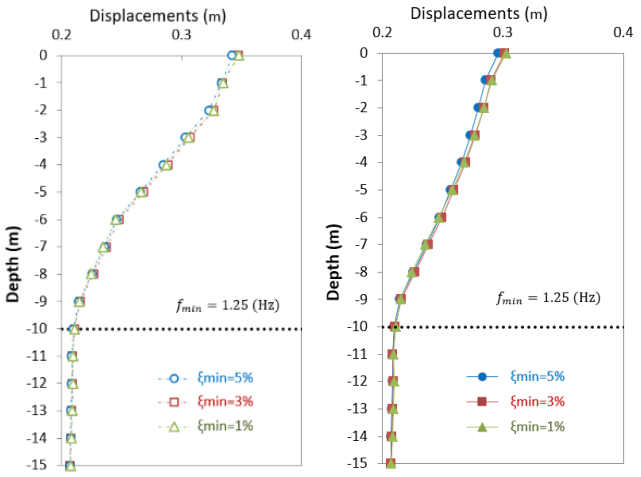

(a) Rigid inclusion system (b) Pile system

Fig. 18. Soil horizontal displacements

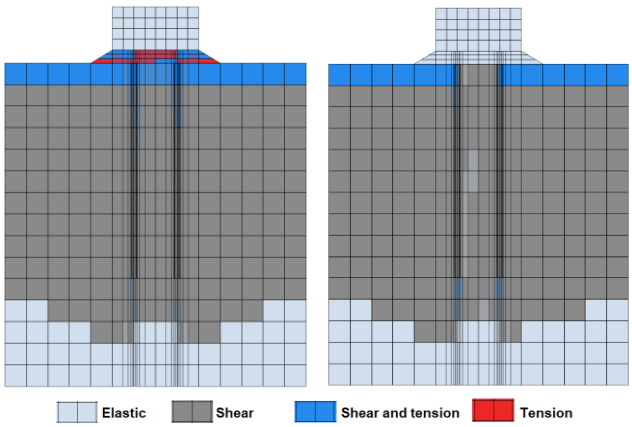

(a) Rigid inclusion system (b) Pile system

Fig. 19 Plastic zones in the systems after loading

the maximum shear stress in the pile and rigid inclusion systems is in the range of 20 kPa for all the cases. At the same time, the strains in the pile system are around 0.6% while in the rigid inclusion systems are greater than 1.5%.

As shown in Fig. 17, there is clearly more energy dissipation for the systems with a lower target damping ratio. In the analyzed systems with the same target damping ratio, larger strains are estimated for the cases analyzed with $f_{min} = 2.0$ Hz than for cases with $f_{min} = 0.75$ Hz. This is because there is in the last one less damping ratio overestimation.

6.3.2 Displacements

The maximum lateral displacements obtained during the completely dynamic loading calculation are presented in this section. The measures are taken vertical to the point that corresponds to the center position of the piled area (Point P in Fig. 3(b)). The horizontal displacements in the soil for the pile and rigid inclusion systems with a target damping ratio of 1%, 3% and 5% and a $f_{min} = 1.25$ Hz under the Loma Prieta earthquake are displayed in Fig. 18. For the other cases, similar results are obtained.

It is visible that the maximum values are obtained in the upper part of the model and decrease with depth for both systems. These results are in accordance to the studies developed by Rahmani and Pak (2012), Kitiyodom et al. (2006) and Liyanapathirana and Poulos (2005). The displacement at the ground surface is around 0.34 m and 0.30 m for the rigid inclusion and pile system respectively. The displacements in the rigid inclusion system are greater from ground surface to 5 m depth than the pile system. This difference is due to the soil energy dissipation and to the interaction between the soil and the rigid elements.

6.3.3 Shearing zones

Fig. 19 presents the zones where plastic strains appear at the end of the dynamic calculation. The systems utilized for this comparison are the pile and rigid inclusion system with a target damping ratio of 5% and a $f_{min} = 1.25$ Hz under the Loma Prieta earthquake.

In the rigid inclusion system, the soft soil is shearing. The earth platform and the zones around the upper inclusion parts (4 m depth) are shearing and others are in a tension state. Similar behavior for the rigid inclusion system is shown in the pile system. Two differences can be noted; the first one is that in the upper part of the pile, there are only shearing zones around the piles until 2 m of depth. The other difference is that there is no shearing of the platform because it is replaced by a slab foundation. The soil under the rigid inclusions and piles (hard soil) is sheared in localized zones.

6.4 Bending moments and normal forces in the rigid vertical elements

In this section, the maximum bending moments and normal forces are presented along the height of the piles and inclusions. In general, the maximum value in the rigid inclusion cases is reached in the middle depth of the elements (5 m) and is null in the top and bottom parts of the vertical elements. The moments along the piles are smaller compared to the rigid inclusions values for depth up to 3 m. However, the values at the elements head are higher in the pile case due to the rigid connection with the foundation slab.

As expected, the moments along the vertical elements are reduced with the increase of the target damping ratio for both pile and rigid inclusion systems (Fig. 20). For example, there is a reduction of about 10% of the moment values from $\xi_{min} = 5\%$ to 1% in the rigid inclusion system with $f_{min} = 1.25$ Hz. In the analyzed cases with $f_{min} = 0.3$ Hz and $f_{min} = 4.0$ Hz, the same comparison induces a decrease of 26%. These values are in accordance with the results presented in section 2.2 which show the damping ratio overestimation for different values of ξ_{min} and f_{min}. For instance, the maximum bending moment of 44 kN.m in the rigid inclusions system with a target damping ratio of 5% and $f_{min} = 1.25$ Hz is reduced to 36 kN.m when the f_{min} is modified to 0.3 Hz due to the damping ratio increase from 5% to 11% (Fig. 12). Similar comparisons can be made in the system with a 3% damping

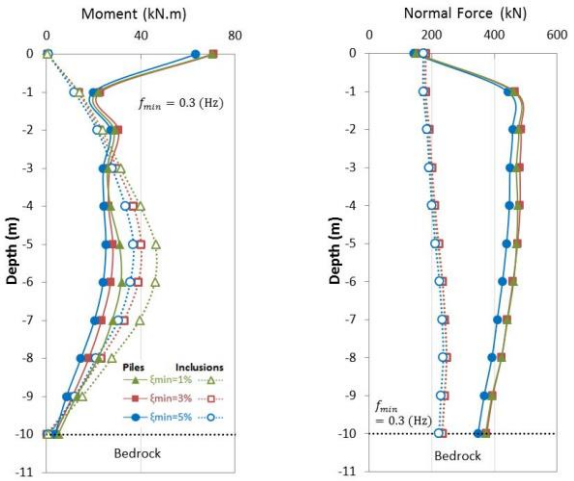

(a) $f_{min} = 0.3(Hz)$

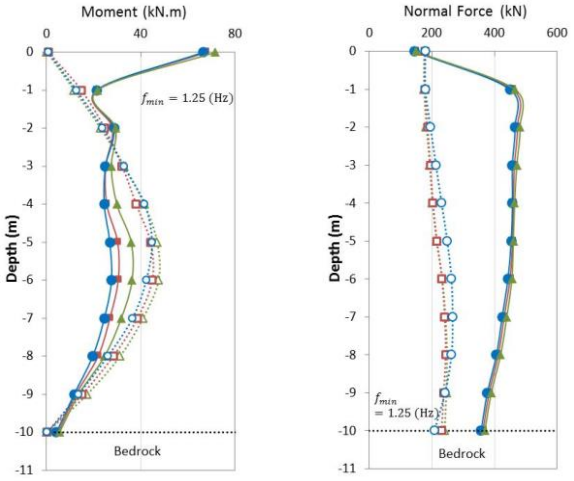

(b) $f_{min} = 1.25(Hz)$

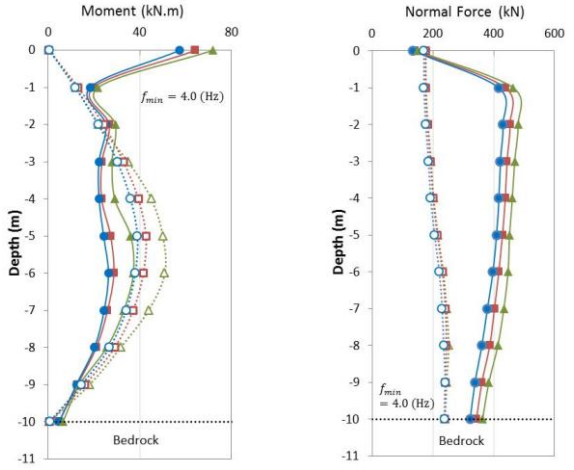

(c) $f_{min} = 4.0(Hz)$

Fig. 20 Maximum bending moments and normal forces in-depth in the pile and rigid inclusion systems for different f_{min} and ξ_{min}

ratio. However, in the systems with a 1% damping ratio, these differences are almost negligible. This means that the differences caused by the damping parameters decrease when the target damping ratio decrease.

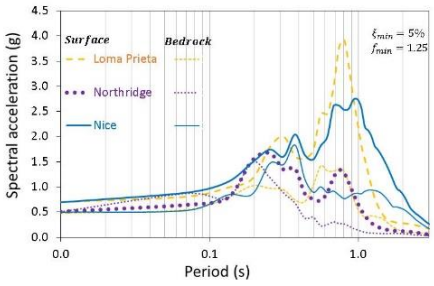

(a) Pile system

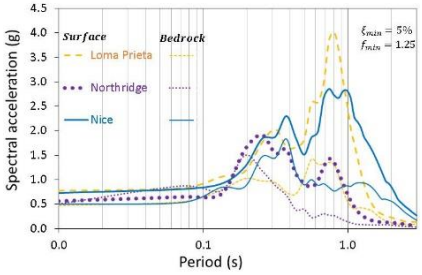

(b) Rigid Inclusion system

Fig. 21 Surface response spectra using Rayleigh damping for different f_{min} values

In the pile systems, the bending moments in the cases of a 5% damping ratio are 16% smaller than the case where $\xi_{min} = 3\%$ for any frequency, and these values are reduced compare to the case where $\xi_{min} = 1\%$ (22% for $f_{min} = 0.3$ Hz and 28% for $f_{min} = 4.0$ Hz). As in the rigid inclusions cases, the values in the piles are influenced by the damping ratio in the system. For example, the maximum bending moment of 66 kN.m at the pile head with a damping ratio of 5% and $f_{min} = 1.25$ Hz is reduced to 57 kN.m when the f_{min} is modified to 4.0 Hz. This is due to the damping ratio increase from 5% to 8.5% (Fig. 12).

From Fig. 20, it can be also noted that the normal forces in the pile cases are greater than in the rigid inclusion ones. The role of the rigid inclusion system is to limit the movement transfer towards the superstructure, which in turn reduces the inertial forces. The variation of the ξ_{min} and f_{min} values in the rigid inclusion cases has a small effect on the normal forces along the elements. Concerning the pile cases, the values in the case with $f_{min} = 1.25$ Hz are almost equal for any damping ratio. However, in the system when $f_{min} = 0.3$ Hz and $f_{min} = 4.0$ Hz, the normal forces are respectively reduced by 6% and 10% for damping ratios of 1% and 5%.

6.5 Influence of the input motion frequency

To study the influence of the frequency on the pile and rigid inclusion systems, the case with $\xi_{min} = 5\%$ and $f_{min} = 1.25$ Hz was analyzed with the Loma Prieta, Northridge and Nice earthquakes. The predominant frequency of each earthquake is shown in Table 2. All the earthquakes were scaled to the same peak ground acceleration.

Fig. 21 shows that the response spectra of the rigid inclusion and pile systems excited with the Loma Prieta

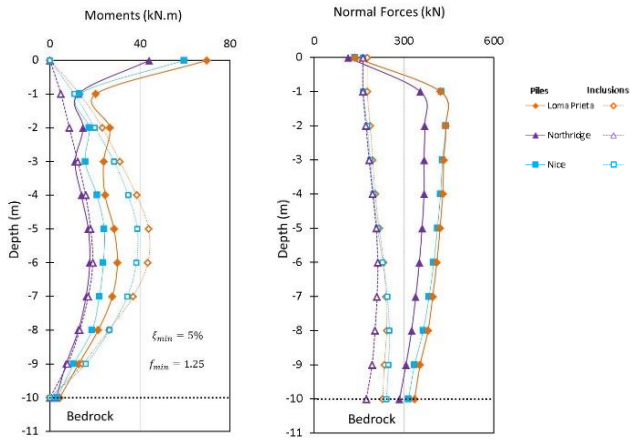

(a) Bending Moments (b) Normal Forces

Fig. 22 Moments and normal forces along elements with input motion frequencies

earthquake are greater in periods from 0.3 to 1.0 s compared to the response obtained with the Northridge and Nice earthquakes. Out of this range, the response of the Nice earthquake is larger. The responses of the rigid inclusion systems are greater than the pile cases.

Fig. 22(a) illustrates that the system analyzed with the Loma Prieta earthquake produces greater bending moments in the pile and rigid inclusion system. Under the Loma Prieta earthquake (1.27 Hz), the damping ratio is equal to 5%. However, this damping ratio increases to 8.3% and 9.3% under the Nice (0.48 Hz) and Northridge (4.3 Hz) earthquakes respectively (Fig. 12). In the rigid inclusion cases, the maximum bending moments (at 5 m depth) obtained under the Loma Prieta earthquake are reduced 11% and 58% compared with the ones of the Nice and Northridge earthquakes respectively. The same comparisons at the pile head give 14% and 36%. These results demonstrate that when the frequency of the input motion is near the f_{min} value, there is no overdamping and the response of the system is greater.

Fig. 22(b) shows that the normal forces in the systems with the Loma Prieta and Northridge earthquakes are almost the same (5% of difference). In the rigid inclusions systems, the values are similar until 6 m depth for all three earthquakes, after that depth, the values of the Northridge are reduced by 5%.

5. Conclusions

In this paper, the main objective is to study the effect of the damping parameters on the response of pile and inclusion through the Rayleigh damping formulation. Soil-pile-structure and soil-inclusion-platform-structure systems are examined. Three-dimensional analyses of both systems are carried out using a finite difference code. A range of values for ξ_{min} and f_{min} are considered. Several earthquakes are used to study the influence of different excitation frequencies.

Developing detailed numerical models to reduce the uncertainties involved in the analysis of soil-pile/inclusions-structure systems, the results of this study, using Rayleigh damping, permit obtaining the following conclusions and recommendations that can be easily applied and adapted for research studies and design of engineering projects.

- When the single control frequency approach is considered in the Rayleigh formulation, it is important to correctly select the central frequency (f_{min}) position to avoid an important overdamping and hence costly conservative design of piles, rigid inclusions or superstructures. The damping ratio should stay close to the target damping ratio.
- In systems with the same target damping ratio, the maximum spectral acceleration at the superstructure base occurs when the system frequency is close to f_{min}. In this case, there is no damping ratio overestimation. However, this difference is negligible when the target damping is reduced. These results show that the superstructure dynamic characteristics have an essential impact when using SSI analysis. Further investigations considering structures with different dynamic characteristics are required.
- Due to the kinematic interaction, the spectral acceleration on the rigid inclusion systems is greater than on the pile ones when considering the same target damping ratio and f_{min}.
- Notable reduction is observed in the bending moments and normal forces along the depth of the vertical elements with the increment of target damping ratio for both pile and rigid inclusion systems. However, it must be considered that the overdamping caused by a change in the damping parameters decreases with the reduction of the target damping ratio.
- When the input motion frequency is close to f_{min}, the overdamping amount is reduced, and the surface spectral acceleration of the analyzed systems increases. Thus, the bending moments and normal forces along the piles and inclusions also increase.
- The influence of ξ_{min} and f_{min} in the shear strains is more evident in the rigid inclusions systems than in the pile ones. Due to the kinematic interaction and the free condition at the rigid inclusion head (or the rigid connection in pile systems), the shear strains in the rigid inclusion systems are larger in the depth range from 0 to 7 m than for the pile cases.
- In order to completely validate the obtained numerical results, experimental studies are necessary.

References

Alsaleh, H. and Shahrour, I. (2009), "Influence of plasticity on the seismic soil-micropiles-structure interaction", *Soil Dyn. Earthq. Eng.*, **29**(3), 574-578. https://doi.org/10.1016/j.soildyn.2008.04.008.

Ambrosini, R.D. (2006), "Material damping vs radiation damping in soil-structure interaction analysis", *Comput. Geotech.*, **33**(2), 86-92. https://doi.org/10.1016/j.compgeo.2006.03.001.

Amorosi, A., Boldini, D. and Elia, G. (2010), "Parametric study on seismic ground response by finite element modelling", *Comput.*

Geotech., **37**(4), 515-528. https://doi.org/10.1016/j.compgeo.2010.02.005.

Banerjee, S., Goh, S.H. and Lee, F.H. (2014), "Earthquake-induced bending moment in fixed-head piles in soft clay". *Géotechnique*, **64**(6), 431-446. https://doi.org/10.1680/geot.12.P.195.

Briançon, L., Dias, D. and Simon, C. (2015), "Monitoring and numerical investigation of a rigid inclusions–reinforced industrial building", *Can. Geotech. J.*, **52**(10), 1592-1604. https://doi.org/10.1139/cgj-2014-0262.

Carbonari, S., Dezi, F. and Leoni, G. (2011), "Linear soil-structure interaction of coupled wall-frame structures on pile foundations", *Soil Dyn. Earthq. Eng.*, **31**(9), 1296-1309. https://doi.org/10.1016/j.soildyn.2011.05.008.

Center for Engineering Strong Motion Data. CESMD. US Geological survey and the California Geological Survey.

Chatterjee, K., Choudhury, D, Dilli, V. and Mukherjee S.P. (2015), "Dynamic analyses and field observation on piles in Kolkata city", *Geomech. Eng*., **8**(3), 415-440.

Chu, D. and Truman, K.Z. (2004), "Effects of pile foundation configurations in seismic soil-pile-structure interaction", *Proceedings of the 13th World Conference on Earthquake Engineering Vancouver*, B.C., Canada.

Eurocode 8 (1998), Design of structures for earthquake resistance - Part 5: Foundations, retaining structures and geotechnical aspects.

Fan, Z., Wang, Y., Xiao, H. and Zhang, C. (2007), "Analytical method of load-transfer of single pile under expansive soil swelling", *J. Central South Univ.*, **14**(4), 575-579. https://doi.org/10.1007/s11771-007-0110-4.

Fathahi, B., Reza Tabatabaiefar, S.H. and Samali, B. (2014), "Soil-structure interaction vs site effect for seismic design of tall buildings on soft soil", *Geomech. Eng.*, **6**(3), 239-320. https://doi.org/10.12989/gae.2014.6.3.293.

Ghorbanzadeh, M., Uygar, E. and Sensoy, S. (2020). "Lateral soil pile structure interaction assessment for semi-active tuned mass damper buildings", *Structures*, **29**(3), 1362-1379. https://doi.org/10.1016/j.istruc.2020.12.020.

Goh, S.H. and Zhang, L. (2017), "Estimation of peak acceleration and bending moment for pile-raft systems embedded in soft clay subjected to far-field seismic excitation", *J. Geotech. Geoenviron. Eng.*, **143**(11), 04017082.1-17. https://doi.org/10.1061/(ASCE)GT.1943-5606.0001779.

Grange S. (2008), "Modélisation simplifiée 3D de l'interaction sol-structure: application au génie parasismique", PhD dissertation, Institut Polytechnique de Grenoble, Grenoble, France. (In French).

Haldar, S. and Babu, S.G.L. (2010), "Failure Mechanisms of pile foundations in liquefiable soil: Parametric study", *Int. J. Geomech.*, **10**(2), 74-84.

Han, Y. (2001), "Dynamic soil-pile-structure interaction". *Proceedings of the International Conferences on Recent Advances in Geotechnical Earthquake Engineering and Soil Dynamics*, **11**, 1-6.

Hashash, Y.M.A. and Park, D. (2002), "Viscous damping formulation and high frequency motion propagation in non-linear site response analysis", *Soil Dyn. Earthq. Eng.*, **22**(7), 611-624. https://doi.org/10.1016/S0267-7261(02)00042-8.

Hatem, A. (2009), " Comportement en zone sismique des inclusions rigides analyse de l'interaction sol-inclusion-matelas de répartition-structure", PhD dissertation, Université des Sciences et Technologies de Lille I, Lille, France. (In French).

Hayashi, Y. and Takahashi, I. (2004), "Soil-structure interaction effects on building response in recent earthquakes". *Proceedings of the 3rd UJNR Workshop on Soil-Structure Interaction*, Menlo Park, California, USA.

Hazzar, L., Hussien, M.N. and Karray, M. (2017), "Influence of vertical loads on lateral response of pile foundations in sands and clays", *J. Rock Mech. Geotech. Eng.*, **9**(2), 291-304. https://doi.org/10.1016/j.jrmge.2016.09.002.

Hokmabadi, A.S., Fatahi, B. and Samali, B., (2014), "Assessment of soil-pile-structure interaction influencing seismic response of mid-rise buildings sitting on floating pile foundations", *Comput. Geotech.*, **55**, 172-186. https://doi.org/10.1016/j.compgeo.2013.08.011.

Houda, M. (2016), "Comportement sous chargement cyclique des massifs de sol renforcés par inclusions rigides : expérimentation en laboratoire et modélisation numérique", PhD dissertation, Université de Grenoble, France. (In French).

Hudson, M., Idriss, I.M. and Beikae, M. (1994), "QUAD4M – A computer program to evaluate the seismic response of soil structures using finite element procedures and incorporating a compliant base", Center for Geotechnical Modeling, Dept. of Civil and Environmental Engineering, UC, Davis.

Idriss, I.M., Lysmer J. Hwang R. and Seed H.B. (1975), "QUAD-4 - A computer program for evaluating the seismic response of soil structures by variable damping finite element procedures", EERC Report 73-16.

Itasca, Flac 3D. (2012), Fast Lagrangian Analysis of Continua in 3-dimentions, version 5.0, manual.

Khanmohammadi, M. and Fakharian, K. (2018), "Evaluation of performance of piled-raft foundations on soft clay: a case of study", *Geomech. Eng.*. **14**(1), 43-50. https://doi.org/10.12989/gae.2018.14.1.043.

Kim, G. Kyung, D., Park, D. and Lee, J. (2015), "CTP-based p-y analysis for mono-piles in sands under static and cyclic loading conditions", *Geomech. Eng*., **9**(3), 313-328. https://doi.org/10.12989/gae.2015.9.3.313.

Kitiyodom, P., Masumoto, T. and Kawaguchi, K., (2006), "Analyses of piled foundations subjected to ground movements induced by tunneling", *Proceedings of the Geotechnical Aspects of Underground Construction in Soft Ground 5th International Symposium*. Amsterdam, Netherlands.

Kuhlemeyer, R.L. and Lysmer, J. (1973), "Finite element method accuracy for wave propagation problems", *J. Soil Mech. Found. Div. - ASCE*, **99**(5), 421-427. https://doi.org/10.1061/JSFEAQ.0001885.

Kumar, A., Choudhury, D. and Katzenbach, R. (2016), "Effect of earthquake on combined pile-raft foundation", *Int. J. Geomech.*, **16**(5), 04016013. https://doi.org/10.1061/(ASCE)GM.1943-5622.0000637.

Kwok, A.O.L. Stewart, J.P. Hashash, Y.M.A., Matasovic, N., Pyke, R., Wang, Z. and Yang, Z. (2007), "Use of exact solutions of wave propagation problems to guide implementation of nonlinear seismic ground response analysis procedures", *J. Geotech. Geoenviron. Eng.*, **133**(11), 1385-1398. https://doi.org/10.1061/(ASCE)1090-0241(2007)133:11(1385).

Liyanapathirana, D.S. and Poulos, H.G., (2005), "Seismic lateral response of piles in liquefying soil", *J. Geotech. Geoenviron. Eng.*, **131**(12), 1466-1479. https://doi.org/10.1061/(ASCE)1090-0241(2005)131:12(1466).

López Jiménez, G.A., Dias, D. and Jenck, O. (2018), "Effect of the soil–pile–structure interaction in seismic analysis: case of liquefiable soils", *Acta Geotechnica*, https://doi.org/10.1007/s11440-018-0746-2.

Lu, X., Li, P., Chen, B. and Chen, Y. (2005), "Computer simulation of the dynamic layered soil-pile-structure interaction system", *Can. Geotech. J.*, **42**(3), 742-751. https://doi.org/10.1139/t05-016.

Luo, C., Yang, X. Zhan, C. Jin, X. And Ding, Z. (2016), "Nonlinear 3D finite element analysis of soil-pile-structure interaction system subjected to horizontal earthquake excitation", *Soil Dyn. Earthq. Eng.*, **84**, 145-156. https://doi.org/10.1016/j.soildyn.2016.02.005.

Lysmer, J. and Kuhlemeyer, R.L. (1969), "Finite dynamic model for infinite media", *J. Eng. Mech. Div. - ASCE*, **95**, 859-878. https://doi.org/10.1061/JMCEA3.0001144

Maheshwari, B.K., Truman, K.Z., El Naggar, M.H. and Gould, P.L. (2004), "Three-dimensional nonlinear analysis for seismic soil-pile-structure interaction", *Soil Dyna. Earthq. Eng.*, **24**, 343-356. https://doi.org/10.1016/j.soildyn.2004.01.001.

Maheshwari, B.K. and Watanabe, H., (2006), "Nonlinear dynamic analysis of pile foundation: effect of separation at soil-pile interface", *Soils Found*, **46**(4), 437-448.

Mánica-Malcom, M.A., Ovando-Shelley, E. and Botero Jaramillo, E. (2016), "Numerical study of the seismic behavior of rigid inclusions in soft Mexico City clay", *J. Earthq. Eng.*, **20**(3), 447-475. https://doi.org/10.1080/13632469.2015.1085462.

Mánica, M., Ovando, E. and Botero, E. (2014), "Assessment of damping models in FLAC", *Comput. Geotech.*, **59**, 12-20. https://doi.org/10.1016/j.compgeo.2014.02.007.

Messioud, S., Okyay, U.S., Sbartai B. and Dias, D. (2016), "Dynamic response of pile reinforced soils and piled foundations", *Geotech. Geol. Eng.*, **34**(3), 789-805. https://doi.org/10.1007/s10706-016-0003-0.

Messioud, S., Sbartai, B. and Dias, D. (2016), "Estimation of dynamic impedance of the soil-pile-slab and soil-pile-mattress-slab systems", *Int. J. Struct. Stab. Dyn.*, **17**(6), 17. https://doi.org/10.1142/S0219455417500572.

Nghiem, H. and Nien-Yin, C. (2008), "Soil-structure interaction effects of high rise buildings", *Proceedings of the 6th International Conference on Case Histories in Geotechnical Engineering*.

Nguyen, Q.V., Fatahi, B. and Hokmabadi, A.S. (2017), "Influence of size and load-bearing mechanism of piles on seismic performance of buildings considering soil-pile-structure interaction", *Int. J. Geomech*., **17**(7), 04017007. https://doi.org/10.1061/(ASCE)GM.1943-5622.0000869.

Okyay, U.S. (2010), "Etude expérimentale et numerique des transferts de charge dans un massif renforcé par inclusions rigides. Application à des cas de chargements statiques et dynamiques", PhD dissertation, L'Institut National des Sciences Appliquées de Lyon. Lyon, France. (In French).

Okyay, U.S., Dias, D., Billion, P. and Vandeputte, D. (2012), "Impedance functions of slab foundations with rigid piles", *Geotech. Geol. Eng.*, **30**(4), 1013-24.

Phillips, C., Hashash, Y.M.A., Oslon, S.M. and Muszyinski, M.R. (2012), "Significance of small strain damping and dilation parameters in numerical modeling of free-field lateral spreading centrifuge tests", *Soil Dyn. Earthq. Eng.*, **42**, 161-176. https://doi.org/10.1016/j.soildyn.2012.06.001.

Phillips, C. and Hashash, Y.M.A. (2009), "Damping formulation for nonlinear 1D site response analyses", *Soil Dyn. Earthq. Eng.*, **29**(7), 1143-1158. https://doi.org/10.1016/j.soildyn.2009.01.004.

Priestley M.J.N. and Grant D.N. (2005). "Viscous damping in seismic design and analysis", *J. Earthq. Eng.*, **9**(2), 229-255.

Rahmani, A. and Pak, A. (2012), "Dynamic behavior of pile foundations under cyclic loading in liquefiable soils", *Comput. Geotech.*, **40**, 114-126. https://doi.org/10.1016/j.compgeo.2011.09.002.

Rajeswari, J.S. and Sarkar, R. (2020), "Estimation of transient forces in single pile embedded in liquefiable soil", *Int. J. Geomech.*, **20**(9), 06020023. https://doi.org/10.1061/(ASCE)GM.1943-5622.0001788.

Rangel-Núñez, J.L., Gomez-Bernal, A., Aguirre-Gonzalez, J., Sordo-Zabay, E. And Ibarra-Razo, E. (2008), "Dynamic response of soft soil deposits improved with rigid inclusions", *Proceedings of the 14th World Conference on Earthquake Engineering* (14WCEE).

Rathje, E.M. and Bray, J.D. (2001), "One- and two-dimensional seismic analysis of solid-waste landfills", *Can. Geotech. J.*, **38**(4), 850-862. https://doi.org/10.1139/t01-009.

Rayhani, M.H. and El Naggar, M.H. (2008), "Numerical modeling of seismic response of rigid foundation on soft soil", *Int. J. Geomech.*, **8**(6), 336-346. https://doi.org/10.1061/(ASCE)1532-3641(2008)8:6(336).

Sadek, M. (2003), "Etude numeriqué du comportement des microspieux sous chargement sismique : analyse de l'effet de groupe er de l'inclinaison", Ph.D. dissertation, Université des Sciences et Technologies de Lille I, Lille, France. (In French).

Sadek, M. and Shahrour, I. (2004), "A three dimensional embedded beam element for reinforced geomaterials", *Int. J. Numer. Anal. Method. Geomech.*, **28**(9), 931-946. https://doi.org/10.1002/nag.357.

Seed, H.B., Romo, M.P., Sun, J.I., Jaime, A. and Lysmer, J. (1988), "The Mexico earthquake of September 19, 1985 - Relationships between soil conditions and earthquake ground motions", *Earthq. Spectra*, **4**(4), 687-729. https://doi.org/10.1193/1.1585498.

Shahrour, I., Alsaleh, H. and Souli, M. (2012), "3D elastoplastic analysis of the seismic performance of inclined micropiles", *Comput. Geotech.*, **39**, 1-7. https://doi.org/10.1016/j.compgeo.2011.08.006.

Shahrour, I., Sadek, M. and Ousta, R. (2001), "Seismic behavior of micropiles used as foundation support elements three-dimensional finite element analysis", *T. Res. Record*, **1772**(1), 84-90. https://doi.org/10.3141/1772-10.

Spears R.E. and Jensen, S.R. (2012), "Approach for selection of Rayleigh damping parameters used for time history analysis", *J. Pressure Vess. Technol.*, **134**, 1-7. https://doi.org/10.1115/1.4006855.

Stewart, J.P., Fenves, G.L. and Seed, R.B. (1999). "Seismic soil-structure interaction in buildings. I: analytical methods", *J. Geotech. Geoenviron. Eng.*, **125**(1), 26-37. https://doi.org/10.1061/(ASCE)1090-0241(1999)125:1(26).

Sun, Q., Bo, J. and Dias, D. (2019), "Viscous damping effects on the seismic elastic response of tunnels in three sites", *Geomech. Eng*., **18**(6), 639-650. https://doi.org/10.12989/gae.2019.18.6.639.

Suwal, S., Pagliaroli, A. and Lanzo, G. (2014), "Comparative study of 1D codes for site response analyses", *Int. J. Landslide Environ.*, **2**(1), 24-31.

Tabatabaiefar, H.R. and Fatahi, B. (2014), "Idealisation of soil-structure system to determine inelastic seismic response of mid-rise building frames", *Soil Dyn. Earthq. Eng.*, **66**, 339-351. https://doi.org/10.1016/j.soildyn.2014.08.007.

Tokimatsu, K., Suzuki, H. and Sato, M. (2005), "Effects of inertial and kinematic interaction on seismic behavior of pile with embedded foundation", *Soil Dynam. Earthq. Eng.*, **25**(7-10), 753-762. https://doi.org/10.1016/j.soildyn.2004.11.018.

Tsai, C.C., Park, D. and Chen, C.W. (2014), "Selection of the optimal frequencies of viscous damping formulation in nonlinear time-domain site response analysis", *Soil Dynam. Earthq. Eng.*, **67**, 353-358. https://doi.org/10.1016/j.soildyn.2014.10.026.

Wang, J.T. (2011), "Investigation of damping in arch dam-water-foundation rock system of Mauvoisin arch dam", *Soil Dynam. Earthq. Eng.*, **31**(1), 33-44. https://doi.org/10.1016/j.soildyn.2010.08.002.

Wolf, J.P. (1985), *Dynamic Soil-Structure Interaction I*. Prentice-Hall, ed., New Jersey: Englewood Cliffs.

Wotherspoon, L.M. (2006), "Three dimensional pile finite element modelling using OpenSees", *Proceedings of the NZSEE Conference*, (Napier).

Wu, G. and Finn, W.D.L. (1997), "Dynamic nonlinear analysis of pile foundations using finite element method in the time domain", *Can. Geotech. J.*, **3**, 44-52. https://doi.org/10.1139/t96-088.

Wu, J.J., Li, Y., Cheng, Q.G., Wen, H. and Liang, X. (2016), "A simplified method for the determination of vertically loaded pile-soil interface parameters in layered soil based on FLAC3D", *Front. Struct. Civil Eng.*, **10**(1), 103-111. https://doi.org/10.1007/s11709-015-0328-4.

Xie, Q., Dinis da Gama, C., Yu, X. And Chen, Y. (2013), "A parametric study of interface characteristics in a buttress retaining wall", *Elec. J. Geotech. Eng.*, **18**, 1477-1492.

Zacek, M. (1996). *Construire parasismique* (In French). Editions Parentheses.

CC